Dynamic structure factor of vitreous silica from first principles:
Comparison to neutron-inelastic-scattering experiments

Alfredo Pasquarello

Institut Romand de Recherche Numérique en Physique des Matériaux (IRRMA), Ecublens, CH-1015 Lausanne, Switzerland
and Department of Condensed Matter Physics, University of Geneva, CH-1211 Geneva, Switzerland

Johannes Sarnthein*

Institut Romand de Recherche Numérique en Physique des Matériaux (IRRMA), Ecublens, CH-1015 Lausanne, Switzerland

Roberto Car

Institut Romand de Recherche Numérique en Physique des Matériaux (IRRMA), Ecublens, CH-1015 Lausanne, Switzerland
and Department of Condensed Matter Physics, University of Geneva, CH-1211 Geneva, Switzerland

(Received 26 January 1998)

Using a first-principles approach, we study the vibrational properties of vitreous SiO_2 which are measured in neutron-scattering experiments. We adopt a model structure consisting of corner-sharing tetrahedra, which was previously generated using first-principles molecular dynamics. We calculate the dynamic structure function $S(q,E)$ as a function of wave vector q and energy E by taking explicitly into account the correlations between different atoms as given by the normal modes. The effects of temperature and finite displacements are also considered. Overall, the agreement with experiment is very good, as illustrated by the comparison for the density of states. However, the calculated and measured $S(q,E)$ differ in some cases up to a factor of 2 in absolute intensity. Nevertheless, the oscillations in $S(q,E)$ describing the correlations between the motions of the atoms are accurately reproduced. The neutron effective density of states obtained directly from $S(q,E)$ yields a good representation of the actual density of states. By introducing a comprehensive scheme, we clarify the relation between neutron and infrared spectra. In particular, we show that the neutron density of states does not distinguish between longitudinal and transverse excitations. Other properties such as the mean-square displacements and the elastic structure factor are also evaluated and found to be in good agreement with experiment. [S0163-1829(98)04422-1]

I. INTRODUCTION

Inelastic neutron scattering provides a powerful tool for investigating the dynamics of disordered network-forming materials.[1–5] The key property measured in these experiments is the scattering function $S(q,E)$ in terms of the wave-vector transfer q and energy transfer E. In disordered systems, the wave vector **q** is not a good quantum number because of the lack of periodicity and a description of the dynamics in terms of dispersion relations between phonon energies and wave vectors does not apply. However, specific information pertaining to the vibrational eigenmodes can still be found in the scattering function. Therefore, in the case of disordered solids, the function $S(q,E)$ plays a crucial role when comparing theoretical models of the dynamics with experiment.

However, theoretical approaches have only rarely attempted to calculate scattering functions of disordered materials,[6–8] in spite of the increasing data obtained by inelastic neutron scattering.[1–5] This stems mainly from the difficulties encountered in reproducing accurate vibrational properties for disordered solids. The uncertainties related to the choice of a structural model and, even more importantly, of reliable interatomic potentials often do not justify pushing the comparison with experiment beyond that for the vibrational density of states.[9–11]

Using a central force model, Sen and Thorpe provided the theoretical framework for the study of vibrational properties of disordered network-forming materials.[12,13] Most subsequent studies were based on molecular-dynamics simulations with classical interaction potentials. In the case of vitreous SiO_2, an improved generation of such potentials was obtained by fitting selected *ab initio* calculations.[14,15] Although these potentials yield structural properties which are consistent with diffraction data, the agreement with experiment for the vibrational density of states is less impressive.[9,11] The accuracy of first-principles approaches in the study of vibrational properties of crystalline solids has been repeatedly established.[16–18] Nevertheless, the application of such techniques to reproduce such properties for amorphous materials has remained far less developed. There are however indications that the accuracy of these techniques would be preserved when applied to disordered solids, as recently demonstrated by our study of vitreous silica.[19,20,23] Using first-principles molecular dynamics,[21,22] we first generated a model structure with good structural and electronic properties.[19] Then, we calculated the corresponding vibrational properties from first principles and found good agreement with experiment also for the neutron vibrational density of states[20] and for the infrared absorption spectrum.[23]

In this paper, we focus on the dynamic structure factor of vitreous silica and calculate within a first-principles scheme various vibrational properties that are directly comparable to data from inelastic neutron scattering.[1,2,5] Since the dynamic

structure factor depends in a more explicit way on the correlations between the atoms than the density of states, the comparison between theory and experiment is more stringent and examines indirectly the accuracy of the vibrational eigenmodes. The dynamic structure factor is evaluated in the harmonic approximation assuming one-phonon scattering events. Debye-Waller and Boson factors are explicitly maintained in the formulas to account for the effects of finite displacements and temperature. In particular, we also calculate the elastic structure factor which is directly measured in neutron-scattering experiments. Finally, we reconstruct the effective neutron density of states from the dynamic structure factor in the same way as it was derived from the experimental results. We discuss differences between the neutron and the actual density of states, and how these relate to the long wavelength limit probed in optical experiments. A preliminary account of the vibrational density of states was already reported previously in a concise form.[20]

This paper is organized as follows. Section II recalls briefly the characteristics of the model structure used in this work.[19] In Sec. III, we describe our approach for obtaining the vibrational frequencies and eigenmodes and discuss the vibrational density of states. In Sec. IV, we calculate the mean-square displacements of all the atoms in our model and use this information to calculate the elastic structure factor. Section V is devoted to the comparison of the dynamic structure factor with experiment. In Sec. VI, the effective neutron density of states is derived and the relation between neutron and infrared spectra clarified. The conclusions are given in Sec. VII.

II. MODEL

The model structure of vitreous silica used in the present study was previously obtained[19] with a quench from the melt using first-principles molecular dynamics.[21,22] The model contains 72 atoms at the experimental density (2.20 g/cm³) in a periodically repeated cubic cell, and consists of a chemically ordered network of corner-sharing tetrahedra. The atomic positions were fully relaxed within density-functional theory, using the local-density approximation for the exchange and correlation energy.[24] Only valence electrons were explicitly retained in our calculation using pseudopotentials to account for core-valence interactions. We used a norm-conserving pseudopotential for silicon[25] and an ultrasoft pseudopotential for oxygen.[26] The electronic wave functions and charge density were described by plane-wave basis sets with cutoffs of 24 and 200 Ry, respectively. The Brillouin zone of the cell was sampled only at the Γ point. A more extended analysis of the structural properties of the model can be found in Ref. 19, whereas a detailed description of the method used for the molecular dynamics and the structural relaxations is given in Ref. 22.

III. VIBRATIONAL DENSITY OF STATES

We make use of the vibrational properties calculated in Ref. 20. The dynamical matrix,

$$D_{i\mu,j\nu} = \frac{1}{\sqrt{m_i m_j}} \frac{\partial^2 V}{\partial r_{i\mu} \partial r_{j\nu}}, \qquad (1)$$
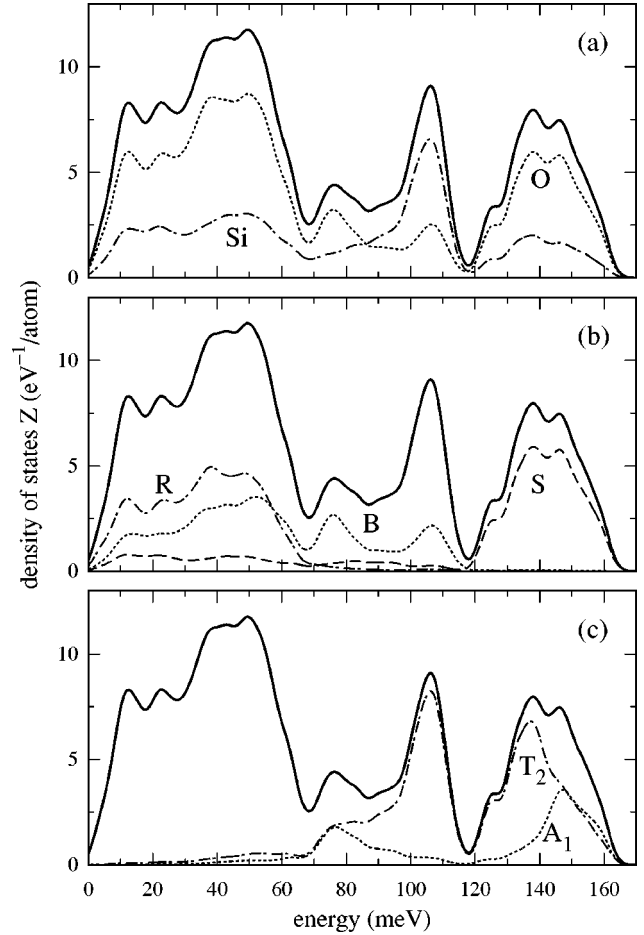
FIG. 1. Vibrational density of states (solid) and decompositions. A Gaussian broadening with $\sigma = 2.5$ meV is used. (a) Partial density of states $Z_\alpha(E)$ for O (dotted line) and Si (dash-dotted line). (b) Decomposition of O motion according to rocking (dot-dashed), bending (dotted), and stretching (dashed) directions. (c) Projection on symmetry-adapted modes of the SiO_4 tetrahedra: T_2 (dash-dotted) and A_1 (dashed).

expressed here in terms of the second derivatives of the total energy V with respect to the atomic displacements $r_{i\mu}$, was calculated numerically by taking finite differences of the atomic forces. In Eq. (1), the indices i and j run over the number of atoms $N = 72$, μ and ν over the Cartesian directions x, y, and z, and m_i is the mass of atom i. By diagonalizing the dynamical matrix

$$\sum_{j\nu} D_{i\mu,j\nu} e_{j\nu}^n = -\omega_n^2 e_{i\mu}^n, \qquad (2)$$

we derive the $3N$ eigenfrequencies ω_n and their corresponding normalized eigenmodes $e_{i\mu}^n$. The normalized vibrational density of states

$$Z(E) = \frac{1}{3N} \sum_n \delta(E - \hbar\omega_n) \qquad (3)$$

is shown in Fig. 1, where a Gaussian broadening with standard deviation $\sigma = 2.5$ meV is used.

In Fig. 1, three different decompositions of the density of states $Z(E)$ allow one to better characterize the vibrational modes. In Fig. 1(a), the density of states is decomposed ac-

cording to the weights of the eigenmodes on the two species, according to $Z(E) = \Sigma_\alpha Z_\alpha(E)$, where the partial density of states $Z_\alpha(E)$ is defined by

$$Z_\alpha(E) = \frac{1}{3N} \sum_{i \subset \alpha}^{N_\alpha} \sum_n |\mathbf{e}_i^n|^2 \delta(E - \hbar \omega_n). \qquad (4)$$

The sum over i is over all the atoms belonging to the species α and $\mathbf{e}_i^n$ corresponds to the displacement vector of atom i with Cartesian components $e_{i\mu}^n$. Figure 1(a) shows that the ratio between the oxygen and the silicon weight is rather close to the concentration ratio throughout the spectrum, indicating that the motions of the two species are strongly correlated. An important exception to this point is the peak at about 106 meV, which is instead dominated by silicon motions.

In Fig. 1(b), the oxygen motion is further decomposed according to the three directions which characterize the local environment, as customary in this field.[27] The peak at lowest energies (below 70 meV) arises mainly from rocking motions in which the O atoms move perpendicular to the Si-O-Si planes formed with their nearest-neighbor Si atoms. The vibrational density of states between 70 and 120 meV is mainly given by O bond-bending motions in the Si-O-Si plane, along the bisector of the Si-O-Si angle. The Si-O stretching motions occurring at higher energy correspond to projections on a direction which is perpendicular to those defined by the bending and rocking motions.

The splitting in the high-frequency doublet has been at the origin of a long-standing debate in the literature.[20] The splitting has alternatively been attributed to two different vibrations of molecular subunits or interpreted as a longitudinal-optic-transverse-optic (LO-TO) effect. In Ref. 20, we solved this issue in favor of the former assignment. In fact, the vibrational density of states as obtained with inelastic neutron experiments is unable to distinguish between transverse and longitudinal excitations, as will be shown in greater detail in Sec. VI. For every SiO$_4$ subunit, the four Si-O stretching modes transform upon rotations as a representation of the symmetry group T_d.[28] Decomposition in irreducible representations yields a nondegenerate representation A_1 and a threefold degenerate representation T_2. The A_1 mode corresponds to an in-phase motion of the four oxygen atoms towards the central Si atom. In the T_2 modes, two oxygen atoms move closer to the central Si atom, while the other two move away. In order to ensure that the modes do not carry an overall translation, the Si atom is immobile in the A_1 mode, but participates in the T_2 modes. In Fig. 1(c), the density of states is projected onto A_1 and T_2 representations.[20] This analysis shows that the origin of the splitting is associated to the different vibrations in the molecular subunits, the low-energy component deriving from T_2 modes and the high-energy one from A_1 modes. This assignment is consistent with the interpretation of infrared measurements,[29] with results from hyper-Raman spectroscopy,[30] and with the comparison between the spectra of the glass and silica polymorphs.[31] It is interesting to note that the peak at 106 meV, which contains a predominant weight of Si motion [see Fig. 1(a)], is mostly T_2 and thus results from the Si response to the Si-O stretching.
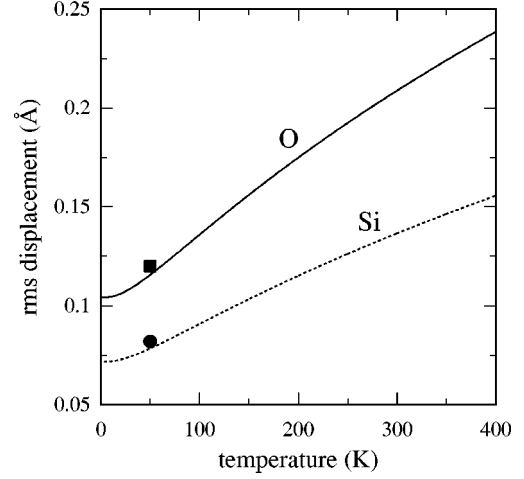
FIG. 2. Root mean-square displacements for oxygen (solid) and silicon atoms (dotted) as a function of temperature. Experimental values for oxygen (square) and silicon (disc) from recent inelastic neutron measurements at 50 K are also shown (Ref. 5).

IV. MEAN-SQUARE DISPLACEMENTS AND ELASTIC STRUCTURE FACTOR

The mean-square displacement of every atom i $\langle \mathbf{u}_i^2 \rangle$ can be calculated in terms of the vibrational energies and eigenmodes:

$$\langle \mathbf{u}_i^2 \rangle = \sum_n \frac{\hbar}{2\omega_n m_i} |\mathbf{e}_i^n|^2 [2 \, n(\hbar \omega_n) + 1], \qquad (5)$$

where the temperature dependence enters through the Boson occupation number $n(E) = [\exp(E/k_B T - 1)]^{-1}$. The root mean-square displacements for oxygen and silicon are given in Fig. 2. In particular, for the zero-point motion we found $\langle \mathbf{u}_{Si}^2 \rangle = 0.005\,16 \pm 0.000\,20$ Å^2 and $\langle \mathbf{u}_O^2 \rangle = 0.010\,88 \pm 0.001\,36$ Å^2. The ratio of the roots of these values is 0.69. This value precisely corresponds to an average value for various crystalline silica polymorphs which is usually taken to obtain experimental values for the mean-square displacements of the two species separately.[32,5] Note that the mean-square displacements of the individual atoms do not differ much from the average values, as indicated by the small standard deviations.

As can be seen from Fig. 2, the calculated values agree well with experimental values obtained from inelastic neutron-scattering measurements at 50 K.[5] In a previous inelastic neutron-scattering experiment at 33 K, Price and Carpenter measured a mean-square displacement averaged over all the atoms in the sample of $\langle \mathbf{u}^2 \rangle = 0.007\,32$ Å^2, slightly lower than the corresponding theoretical value of 0.009\,88 Å^2. By fitting the self scattering at room temperature, Wright and Sinclair measured an average mean-square displacement of 0.0121 Å^2, significantly smaller than our theoretical value of 0.0350 Å^2 for room temperature. At present this difference remains unexplained.

The mean-square displacements can be approximated by a formula which does not contain an explicit dependence on the eigenmodes:
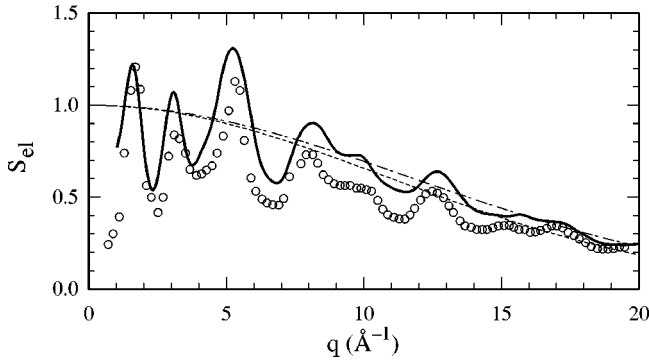
FIG. 3. Elastic structure factor $S_{el}(q)$ (solid) calculated for 50 K compared to the experimental one (open circles) measured at the same temperature (Ref. 5). The dash-dotted curve corresponds to $\exp(-q^2\langle\mathbf{u}^2\rangle/3)$, where $\langle\mathbf{u}^2\rangle=0.01097$ Å^2 is the theoretical mean-square displacement averaged over all the atoms. The dashed curve shows the same function with the experimental value of $\langle\mathbf{u}^2\rangle=0.01263$ Å^2 (Ref. 5).

$$\langle\mathbf{u}_i^2\rangle\cong\sum_n\frac{\hbar}{2\omega_n m_i N}[2\,n(\hbar\omega_n)+1]$$

$$=\frac{3\hbar^2}{2m_i}\int dE\,\frac{2\,n(E)+1}{E}Z(E), \tag{6}$$

where explicit use was made of the definition of the density of states in Eq. (3). When this formula is used to calculate the average mean-square displacement for our model vitreous silica, this approximation appears to reproduce the exact average within a couple of percent. This provides support to the practice of extracting a value for the mean-square displacement from Eq. (6),[2–4] provided a reasonable estimate for the density of states $Z(E)$ is known.

Once the equilibrium positions $\mathbf{R}_i$ and the corresponding mean-square displacements $\langle\mathbf{u}_i^2\rangle$ are known, the elastic structure factor can be derived:[33,2]

$$S_{el}(\mathbf{q})=\frac{1}{N}\sum_{ij}\frac{b_ib_j}{\langle b^2\rangle}e^{-(W_i+W_j)}\,e^{i\mathbf{q}\cdot(\mathbf{R}_i-\mathbf{R}_j)}, \tag{7}$$

where b_i are the neutron-scattering lengths,

$$\langle b^2\rangle=\frac{1}{N}\sum_i b_i^2, \tag{8}$$

and W_i are Debye-Waller factors which for an isotropic amorphous system are given by

$$W_i(q)=q^2\langle\mathbf{u}_i^2\rangle/6. \tag{9}$$

We took $b_{Si}=4.149$ fm for Si atoms and $b_O=5.805$ fm for O atoms.[2]

The elastic structure factor $S_{el}(q)$, calculated by taking a spherical average of $S_{el}(\mathbf{q})$ over the directions of $\mathbf{q}$, is compared to the experimental one in Fig. 3.[5] The theoretical curve and the experimental data were both obtained for a temperature of 50 K. The agreement is very good. The experimental data decay slightly faster with q, as a consequence of the small difference in the average mean-square displacements found between theory ($\langle\mathbf{u}^2\rangle=0.01097$ Å^2)

and experiment ($\langle\mathbf{u}^2\rangle=0.01263$ Å^2).[5] This is illustrated in Fig. 3 by the corresponding functions $\exp(-2\bar{W})$, where

$$\bar{W}=q^2\langle\mathbf{u}^2\rangle/6. \tag{10}$$

V. NEUTRON-SCATTERING FUNCTION

Since Si and O have negligible incoherent scattering cross sections, the one-phonon neutron-scattering function is given by[2,33]

$$S(\mathbf{q},E)=\frac{1}{N\langle b^2\rangle}\sum_{ii'}b_ib_{i'}e^{-(W_i+W_{i'})}e^{i\mathbf{q}\cdot(\mathbf{R}_{i'}-\mathbf{R}_i)}$$

$$\times\sum_n\hbar\frac{(\mathbf{q}\cdot\mathbf{e}_i^n)^*(\mathbf{q}\cdot\mathbf{e}_{i'}^n)}{2(m_im_{i'})^{1/2}\omega_n}[n(\hbar\omega_n)+1]\,\delta(E-\hbar\omega_n). \tag{11}$$

The notation adopted in this work is close to that in Ref. 2, to which we refer for a more detailed formulation of the neutron-scattering theory.

In Figs. 4 and 5, the calculated $S(q,E)$, obtained from $S(\mathbf{q},E)$ by a spherical average over the $\mathbf{q}$ directions, is compared to available experimental data from inelastic neutron scattering.[1,5] The theoretical calculations were carried out for a temperature of 0 K.[35] There are two sets of experimental data in the literature. The earliest data were obtained by Carpenter and Price at a temperature of 33 K.[1] We reproduce here the $S(q,E)$ for transferred energies of 49.2, 98.5, and 145.7 meV, corresponding to peaks in the neutron density of states. More recently the neutron-scattering experiment was repeated at a temperature of 50 K with a higher energy resolution.[5] The $S(q,E)$ functions from this experiment are also reported in Figs. 4 and 5 for energies of 15, 50, 67, 100, and 133 meV. Whereas the former experimental data are reproduced with their original units, we were unable to deduce the units for $S(q,E)$ from Ref. 5. The data from the latter experiment are therefore reproduced with a single arbitrary scaling factor.

In absolute terms, the theoretical curves generally underestimate the data measured by Carpenter and Price, with differences up to a factor of 2. The agreement between theory and experiment is far better when one considers the oscillations of the scattering function, which are a direct manifestation of the coherent scattering of atoms. In particular, the correspondence with the more recent data obtained with a higher energy resolution is remarkable.[5] This accord also provides further support in favor of the structural model for vitreous silica consisting of a network of corner-sharing tetrahedra.

For comparison, we also give in Figs. 4 and 5 the scattering function in the extreme incoherent approximation:[2]

$$S_i(q,E)=e^{-2\bar{W}}\frac{\hbar^2q^2}{2\bar{m}E}[n(E)+1]\,Z(E), \tag{12}$$

where $\bar{m}^{-1}=\Sigma_im_i^{-1}/N$. In this approximation, the oscillations in the scattering function disappear. However, the intensity and the dependence on q are well approximated. The incoherent approximation presents significant deviations
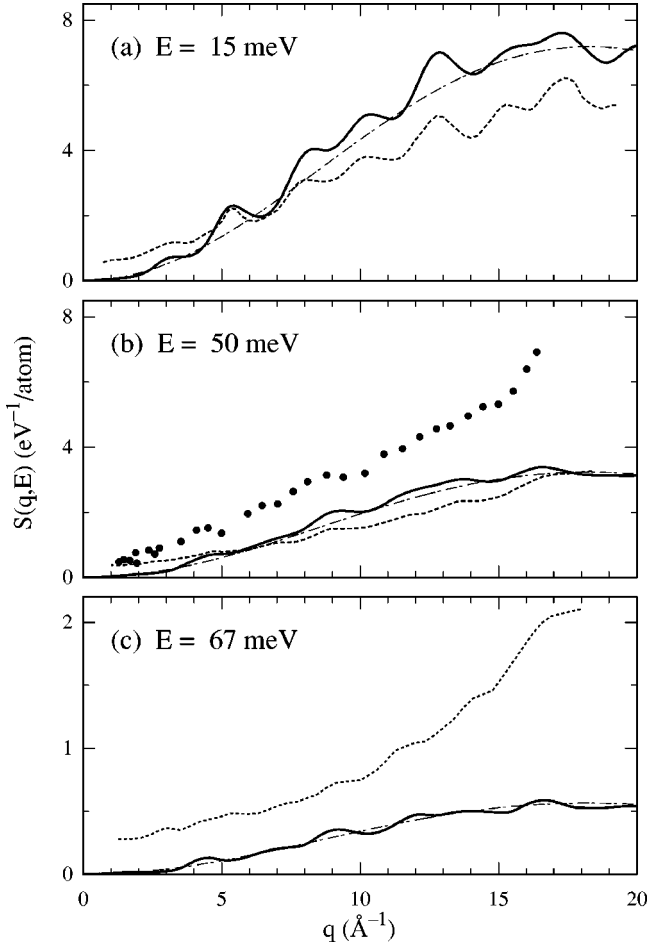
FIG. 4. Coherent one-phonon dynamic structure factor $S(q,E)$ calculated at 0 K (solid) for three different values of E: (a) $E=15$ meV, (b) $E=50$ meV, and (c) $E=67$ meV. The dynamic structure factor $S_i(q)$ in the incoherent approximation is also shown (dash-dotted). The discs in (b) correspond to inelastic neutron-scattering data from Ref. 1 measured at 33 K. The dashed curves correspond to more recent neutron data obtained at 50 K (Ref. 5) and are reproduced here by scaling the values by a single arbitrary constant.

The expression for the incoherent scattering function is also useful to define a generalized density of states in terms of the coherent scattering function:[2]

$$G(q,E) = e^{2\bar{W}} \frac{2\bar{m}E}{\hbar^2 q^2} \frac{1}{n(E)+1} S(q,E). \qquad (13)$$

The oscillations as a function of q are more pronounced in $G(q,E)$ than in $S(q,E)$, where they are masked by the strong $q^2 \exp(-2\bar{W})$ dependence. In Fig. 6, calculated $G(q,E)$ for various energies E are compared to the static structure factor $S(q)$ obtained previously for the same model.[19] At $E=15$ meV, it was found experimentally that the phase of the oscillations coincided with that of $S(q)$, but that the first sharp diffraction peak (FSDP) had disappeared.[5] Our theoretical results confirm this observation. In fact, besides the disappearance of the FSDP, not only the phase but
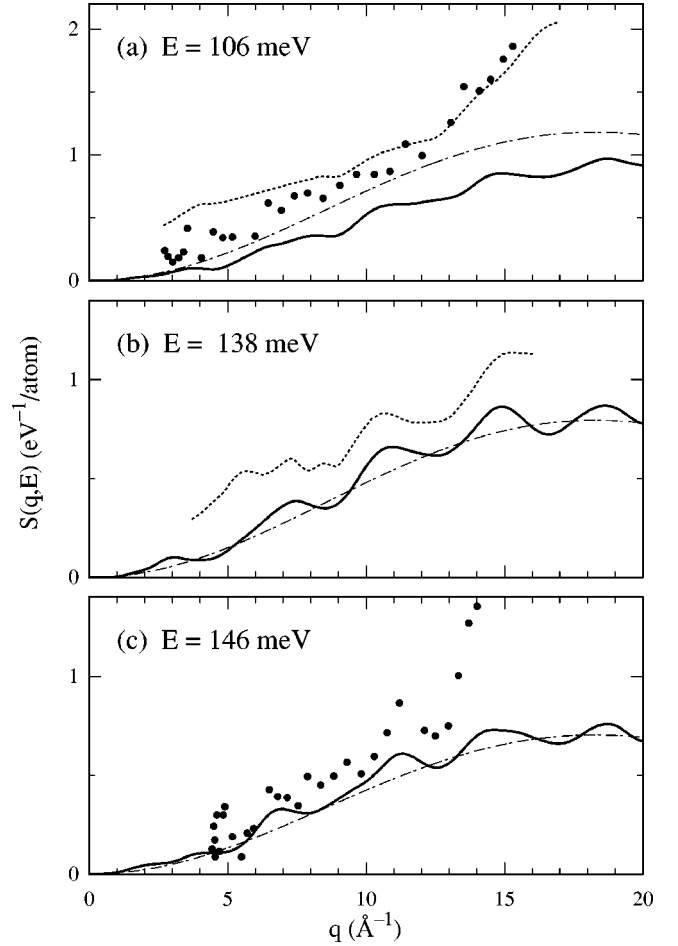
FIG. 5. Coherent one-phonon dynamic structure factor $S(q,E)$ calculated at 0 K (solid) for three different values of E: (a) $E=106$ meV, (b) $E=138$ meV, and (c) $E=146$ meV, which correspond to the principal features in the high-energy part of the spectrum. Notations as in Fig. 4. The data from Ref. 5 are reproduced with the same scaling constant as in Fig. 4.

also the overall shape of $G(q,E)$ at $E=15$ meV resembles $S(q)$ very closely. The physical reasons for this resemblance and for the disappearance of the FSDP remain unclear. At $E=50$ meV, we found that the oscillation is out of phase with respect to $S(q)$, in good agreement with the experimental observations.[5] We also calculated $G(q,E)$ for $E=138$ meV and $E=146$ meV, which correspond to the peak values of the high-energy doublet in the density of states. In the attempt to understand the nature of the splitting, the two components were measured separately, but were not found to show marked differences.[5] This is consistent with the results in Fig. 6 which show that $G(q,E)$ at $E=138$ meV and $E=146$ meV differ appreciably only for low q values.

VI. EFFECTIVE NEUTRON DENSITY OF STATES

The effective neutron density of states $G(E)$ is obtained by averaging the generalized density of states $G(q,E)$ over q:[2]

only at $E=106$ meV, which corresponds to the peak in the density of states with a predominant contribution of Si motion.

$$G(E) = \frac{\int_{q_1}^{q_2} dq\, G(q,E)}{q_2 - q_1}. \qquad (14)$$
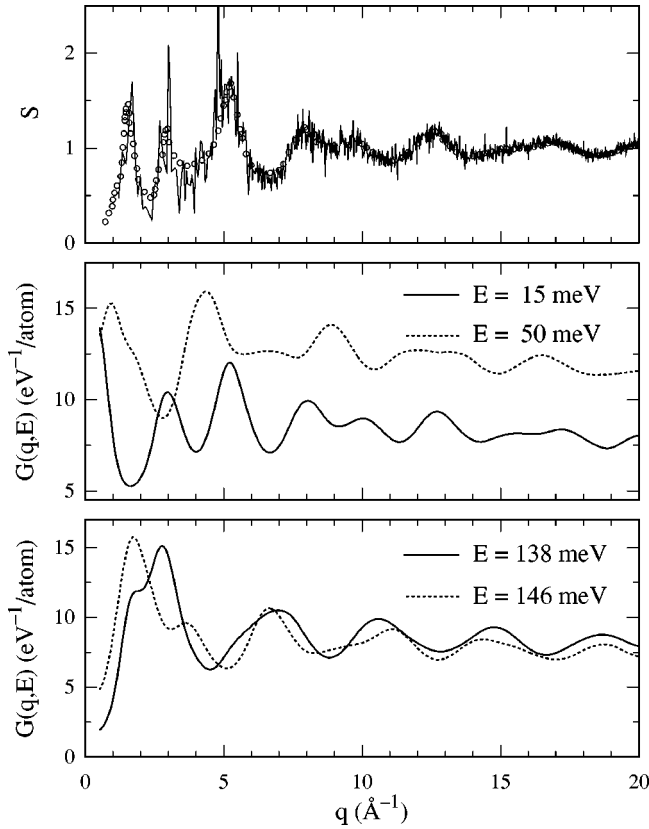
FIG. 6. Generalized density of states $G(q,E)$ calculated at a temperature of 50 K for various energies and compared to the static structure factor $S(q)$, previously obtained in Ref. 19 for the same model. The open circles in the upper panel are neutron-diffraction data from Ref. 34.

We calculated $G(E)$ for a temperature of 33 K with $q_1 = 6$ Å^{-1} and $q_2 = 13$ Å^{-1}, in the same conditions as in the experiment of Carpenter and Price.[1,2] Very good agreement is found between theory and experiment as can be seen from
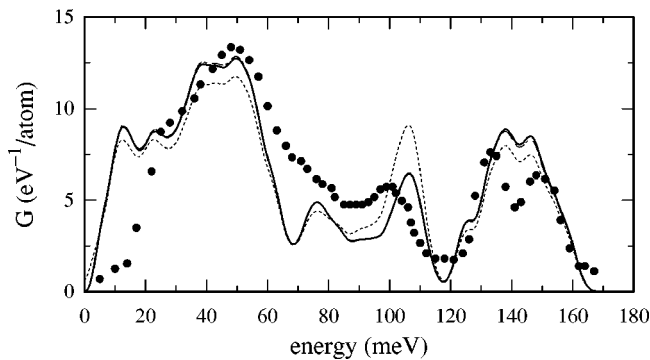
FIG. 7. Effective neutron density of states $G(E)$ (solid) compared to the actual density of states $Z(E)$ (dashed). The experimental $G(E)$ obtained in Ref. 1 by inelastic neutron scattering is also shown (discs). In the same way as in the experiment, the calculated $G(E)$ is obtained at a temperature of 33 K and by averaging the wave vectors q between 6 and 13 Å^{-1}. We also show the effective transverse density of states $G_\perp(E)$ (dot-dashed) obtained by averaging over the same wave vectors the transverse generalized density of states $G_\perp(q,E)$: The longitudinal $G(E)$ (solid) and the transverse $G_\perp(E)$ (dot-dashed) are almost indistinguishable on the scale of the figure.
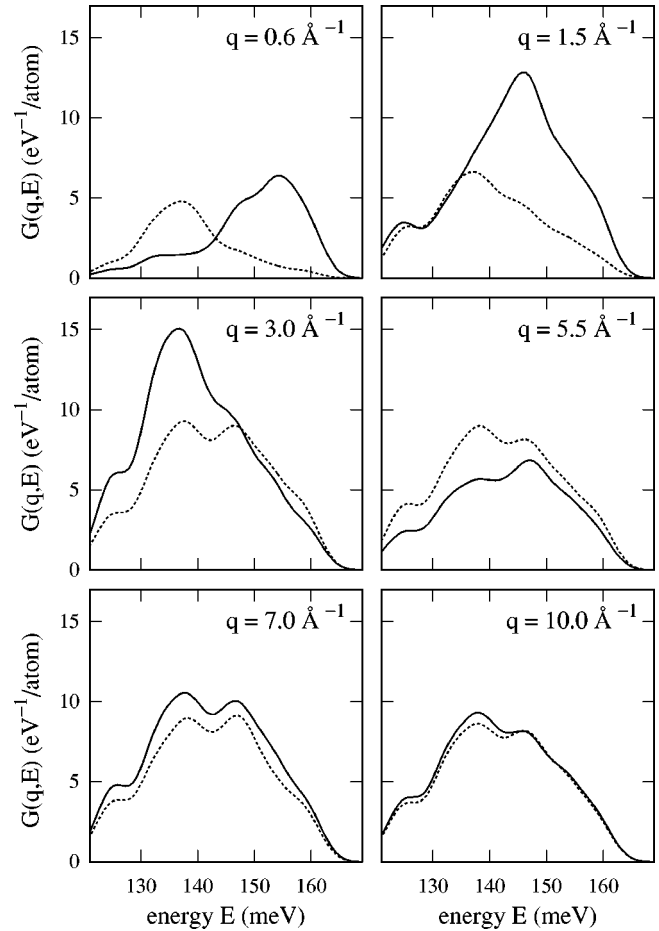
FIG. 8. Longitudinal [$G(q,E)$, solid] and transverse dynamic structure factors [$G_\perp(q,E)$, dashed] for different values of the wave vector q, in the Si-O stretching regime. The curves are obtained for a temperature of 0 K.

Fig. 7. The actual density of states $Z(E)$ is also added for comparison. For vitreous silica, $Z(E)$ and $G(E)$ do not differ dramatically. A significant difference is only observed at 106 meV where $G(E)$ underestimates the actual density of states. This underestimation is balanced by an overestimation throughout the rest of the spectrum. The difference between $Z(E)$ and $G(E)$ at 106 meV should be related to the worse agreement between the scattering function and its incoherent approximation at this energy. Note that the $G(E)$ in Fig. 7 is almost equal to that obtained in Ref. 20, where Debye-Waller factors and Boson factors were omitted. This implies that the dependence on temperature and finite displacements is not crucial in the definition of $G(q,E)$ in Eq. (13).

The differences between neutron and infrared spectra[36,37,29] has given rise to confusion in the literature and in some cases to erroneous interpretations.[20] It is well known that in the limit of long wavelengths ($q \rightarrow 0$), which is probed in optical experiments, important LO-TO splittings arise because of the long-range nature of the electric field.[38] The role of longitudinal and transverse excitations in the neutron spectrum is less well understood.

In order to clarify the relation between the neutron and the infrared spectra we introduce the *transverse* generalized density of states $G_\perp(\mathbf{q},E)$:

$$G_\perp(\mathbf{q},E) = e^{2\bar{W}} \frac{2\bar{m}E}{\hbar^2} \frac{1}{n(E)+1} \frac{1}{N\langle b^2 \rangle}$$

$$\times \frac{1}{2}\sum_{ii'\lambda} b_i b_{i'} e^{-(W_i+W_{i'})} e^{i\mathbf{q}\cdot(\mathbf{R}_{i'}-\mathbf{R}_i)}$$

$$\times \sum_n \hbar \frac{(\hat{\mathbf{q}}_\lambda^\perp \cdot \mathbf{e}_i^n)^*(\hat{\mathbf{q}}_\lambda^\perp \cdot \mathbf{e}_{i'}^n)}{2(m_i m_{i'})^{1/2}\omega_n}$$

$$\times [n(\hbar\omega_n)+1]\delta(E-\hbar\omega_n), \qquad (15)$$

where $\hat{\mathbf{q}}_\lambda^\perp$ (for $\lambda=1,2$) are two unit vectors which are orthogonal to the direction of $\mathbf{q}$ and to each other. For every $\mathbf{q}$, $G_\perp(\mathbf{q},E)$ results from the average over the two transverse directions $\hat{\mathbf{q}}_\lambda^\perp$. In the following we only consider $G_\perp(q,E)$ which is obtained as a spherical average over the directions of $\mathbf{q}$. If one replaces the unit vectors $\hat{\mathbf{q}}_\lambda^\perp$ in Eq. (15) by the unit vector $\hat{\mathbf{q}}$ in the direction of $\mathbf{q}$ and performs the spherical average over the directions of $\mathbf{q}$, one recovers the same $G(q,E)$ previously defined in Eq. (13). Therefore $G(q,E)$ and $G_\perp(q,E)$ act as the neutron counterparts of the longitudinal and transverse dielectric response functions defined by De Leeuw and Thorpe.[38]

In Fig. 8, the generalized density of states $G(q,E)$ and $G_\perp(q,E)$ are shown for different values of q in the part of the spectrum corresponding to the stretching modes. In the limit of small q,[39] the transverse and the longitudinal spectra show peaks at distinct energy positions. This correponds to what is observed in infrared measurements, with the caveat that the infrared intensities are modulated by the dynamic charges rather than by the neutron-scattering lengths.[23] In the limit of large q the distinction between $G(q,E)$ and $G_\perp(q,E)$ vanishes, both spectra showing a double-peak structure.

The effective neutron density of states is obtained by averaging wave vectors which are significantly larger than those probed in infrared experiments. We averaged $G_\perp(q,E)$ over the same wave-vector range as in the experiment of Carpenter and Price ($6<q<13$ Å^{-1}), obtaining an effective

transverse density of states $G_\perp(E)$. We included this transverse density in Fig. 7, where it is compared with the (longitudinal) $G(E)$. The two spectra are hardly distinguishable. Thus, typical neutron experiments are carried out in a regime of wave vectors where the differences between longitudinal and transverse excitations have essentially vanished.

VII. CONCLUSIONS

Using a first-principles approach, we calculated a series of vibrational properties of vitreous silica which are directly measurable by neutron scattering and performed a close comparison between theory and experiment. In this study, we adopted a model structure which was previously generated using first-principles molecular dynamics.[19] The properties which we calculated included the mean-square displacements, the elastic structure factor, the dynamic structure factor, and the effective density of states. Overall the agreement with experiment was very good. In particular, the effective neutron density of states was well reproduced by our theory. However, calculated and measured dynamic structure factors showed differences in absolute intensity. Nevertheless, the oscillations as a function of q, which are a specific feature of the correlations between the atoms, were accurately reproduced in our model. Furthermore, this study clarified the relation between neutron and infrared spectra. A comprehensive scheme was developed which accounts for the appearance of LO and TO excitations in the limit of small wave vectors (as probed in infrared experiments), and which shows how the distinction between LO and TO spectra vanishes when larger wave vectors are probed (as in typical neutron measurements).

*Present address: Institute for Neuroinformatics, ETH, Gloriastrasse 30, CH-8006 Zurich, Switzerland.

[1] J.M. Carpenter and D.L. Price, Phys. Rev. Lett. **54**, 441 (1985).

[2] D.L. Price and J.M. Carpenter, J. Non-Cryst. Solids **92**, 153 (1987).

[3] U. Walter, D.L. Price, S. Susman, and K.J. Volin, Phys. Rev. B **37**, 4232 (1988).

[4] M. Arai, D.L. Price, S. Susman, K.J. Volin, and U. Walter, Phys. Rev. B **37**, 4240 (1988).

[5] M. Arai, A.C. Hannon, A.D. Taylor, T. Otomo, A.C. Wright, R.N. Sinclair, and D.L. Price, Trans. Am. Crystallogr. Assoc. **27**, 113 (1991); M. Arai, A.C. Hannon, A.D. Taylor, A.C. Wright, R.N. Sinclair, and D.L. Price, in *The Physics of Non-Crystalline Solids*, edited by L.D. Price, W.C. La Course, and H.J. Stevens (Taylor and Francis, London, 1992), p. 479; Physica B **180 & 181**, 779 (1992); A.C. Hannon, M. Arai, R.N. Sinclair, and A.C. Wright, J. Non-Cryst. Solids **150**, 239 (1992).

[6] See references in S.R. Elliott, *Physics of Amorphous Materials*, 2nd ed. (Longman, London, 1990).

[7] W. Jin, P. Vashishta, R.K. Kalia, and J.P. Rino, Phys. Rev. B **48**, 9359 (1993).

[8] R.L. Cappelletti, M. Cobb, D.A. Drabold, and W.A. Kamitakahara, Phys. Rev. B **52**, 9133 (1995); M. Cobb, D.A. Drabold, and R.L. Cappelletti, *ibid.* **54**, 12 162 (1996).

[9] R.G. Della Valle and E. Venuti, Chem. Phys. **179**, 411 (1994).

[10] M. Wilson, P.A. Madden, M. Hemmati, and C.A. Angell, Phys. Rev. Lett. **77**, 4023 (1996).

[11] K. Vollmayr, W. Kob, and K. Binder, Phys. Rev. B **54**, 15 808 (1996).

[12] P.N. Sen and M.F. Thorpe, Phys. Rev. B **15**, 4030 (1977).

[13] F.L. Galeener, Phys. Rev. B **19**, 4292 (1979).

[14] S. Tsuneyuki, M. Tsukada, H. Aoki, and Y. Matsui, Phys. Rev. Lett. **61**, 869 (1988).

[15] B.W.H. van Beest, G.J. Kramer, and R.A. van Santen, Phys. Rev. Lett. **64**, 1955 (1990).

[16] P. Giannozzi, S. de Gironcoli, P. Pavone, and S. Baroni, Phys. Rev. B **43**, 7231 (1991).

[17] X. Gonze, D.C. Allan, and M.P. Teter, Phys. Rev. Lett. **68**, 3603 (1992).

[18] A. Dal Corso, A. Pasquarello, and A. Baldereschi, Phys. Rev. B **56**, R11 369 (1997).

[19] J. Sarnthein, A. Pasquarello, and R. Car, Phys. Rev. Lett. **74**, 4682 (1995); Phys. Rev. B **52**, 12 690 (1995).

[20] J. Sarnthein, A. Pasquarello, and R. Car, Science **275**, 1925 (1997).

[21] R. Car and M. Parrinello, Phys. Rev. Lett. **55**, 2471 (1985).

[22] A. Pasquarello, K. Laasonen, R. Car, C. Lee, and D. Vanderbilt, Phys. Rev. Lett. **69**, 1982 (1992); K. Laasonen, A. Pasquarello, R. Car, C. Lee, and D. Vanderbilt, Phys. Rev. B **47**, 10 142 (1993).

[23] A. Pasquarello and R. Car, Phys. Rev. Lett. **79**, 1766 (1997).

[24] We used formulas given in J.P. Perdew and A. Zunger, Phys. Rev. B **23**, 5048 (1981).

[25] G.B. Bachelet, D.R. Hamann, and M. Schlüter, Phys. Rev. B **26**, 4199 (1982).

[26] D. Vanderbilt, Phys. Rev. B **41**, 7892 (1990).

[27] R.J. Bell, P. Dean, and D.C. Hibbins-Butler, J. Phys. C **4**, 1214 (1971); R.J. Bell and D.C. Hibbins-Butler, *ibid.* **8**, 787 (1975).

[28] The narrow O-Si-O distribution (see Ref. 19) ensures that this assumption is a very good approximation.

[29] C.T. Kirk, Phys. Rev. B **38**, 1255 (1988).

[30] V.N. Denisov, B.N. Mavrin, V.B. Podobedov, Kh.E. Sterin, and B.G. Varshal, J. Non-Cryst. Solids **64**, 195 (1984).

[31] P. McMillan, B. Piriou, and A. Navrotsky, Geochim. Cosmochim. Acta **46**, 2021 (1982); P.F. McMillan, P.T. Poe, Ph. Gillet, and B. Reynard, *ibid.* **58**, 3653 (1994).

[32] A.C. Wright and R.N. Sinclair, J. Non-Cryst. Solids **76**, 351 (1985).

[33] D.L. Price and K. Sköld, in *Neutron Scattering*, edited by K. Sköld and D.L. Price (Academic, Orlando, 1986), p. 1.

[34] S. Susman, K.J. Volin, D.L. Price, M. Grimsditch, J.P. Rino, R.K. Kalia, P. Vashishta, G. Gwanmesia, Y. Wang, and R.C. Liebermann, Phys. Rev. B **43**, 1194 (1991).

[35] The function $S(q,E)$ calculated at 0 K and showed in Figs. 4 and 5 differs only slightly from those calculated at 33 K and 50 K, on the scale set by the differences between the calculated and measured $S(q,E)$.

[36] F.L. Galeener and G. Lucovsky, Phys. Rev. Lett. **37**, 1474 (1976).

[37] F.L. Galeener, A.J. Leadbetter, and M.W. Stringfellow, Phys. Rev. B **27**, 1052 (1983).

[38] S.W. de Leeuw and M.F. Thorpe, Phys. Rev. Lett. **55**, 2879 (1985); M.F. Thorpe and S.W. de Leeuw, Phys. Rev. B **33**, 8490 (1986).

[39] The smallest wave vector allowed by our cell size, which does not require depolarizing fields (Ref. 38), is $q = 0.6$ Å^{-1}.